

Initial fluctuation effects on harmonic flows in high-energy heavy-ion collisions

L. X. Han,^{1,2} G. L. Ma,¹ Y. G. Ma,^{1,*} X. Z. Cai,¹ J. H. Chen,¹ S. Zhang,¹ and C. Zhong¹

¹*Shanghai Institute of Applied Physics, Chinese Academy of Sciences, Shanghai 201800, China*

²*Graduate School of the Chinese Academy of Sciences, Beijing 100080, China*

(Dated: February 17, 2022)

Within the framework of a multi-phase transport model, harmonic flows v_n ($n = 2, 3$ and 4) are investigated for Au + Au collisions at $\sqrt{s_{NN}} = 200$ GeV and Pb + Pb collisions at $\sqrt{s_{NN}} = 2.76$ TeV. The event-by-event geometry fluctuations significantly contribute to harmonic flows. Triangular flow (v_3) originates from initial triangularity (ε_3) and is developed by partonic interactions. The conversion efficiency (v_n/ε_n) decreases with harmonic order and increases with partonic interaction cross section. A mass ordering in the low p_T region and number of constituent quark scaling in the middle p_T region seem to work roughly for n -th harmonic flows at both energies. All features of harmonic flows show similar qualitative behaviors at RHIC and LHC energies, which implies that the formed partonic matters are similar at the two energies.

PACS numbers: 12.38.Mh, 11.10.Wx, 25.75.Dw

I. INTRODUCTION

Results from the Brookhaven Relativistic Heavy-Ion Collider (RHIC) indicate that a strongly-interacting partonic matter has been created in relativistic nucleus-nucleus collisions [1]. A powerful probe exposing the characteristics of new matter, elliptic flow, has been measured via the second Fourier coefficient (v_2) in the azimuthal distribution of final particles. It is translated from an early stage coordinate space asymmetry, which can reflect how the hot matter evolves hydrodynamically [1–3]. The v_2 data show remarkable hydrodynamical behaviors, which implies the formed matter is thermalized in a very short time and expands collectively as a perfect-like liquid with a very small shear viscosity over entropy density ratio (η/s) [4–7]. Elliptic flow (v_2) has been studied widely as functions of centrality, transverse momentum (p_T) and pseudorapidity (η) etc. A mass-ordering at low p_T and a Number of Constituent Quark (NCQ) scaling at intermediate p_T for v_2 have been observed, which suggests that a thermalized partonic matter is formed and a collective motion is developed prior to hadronization [8–12]. On the other hand, a geometry (participant eccentricity) scaling was observed for v_2 fluctuations, which implies not only participant eccentricity is responsible for elliptic flow, but also the event-by-event initial state geometry fluctuations contribute to harmonic flow [13–15].

It has been recently found that the triangular flow (v_3) is not zero in the azimuthal distribution of final particles. In fact, because of the non-smooth profile, coming from the event-by-event fluctuations of participant nucleons, it shows a triangular initial geometry shape can be transferred into momentum space by hydrodynamical evolution. In recent studies, it has been demonstrated

that triangular flow significantly contributes on the near-side ridge and away-side double bumps in two-particle azimuthal correlations [16, 17]. As a new probe, triangular flow is believed to provide more information about the formed hot and dense matter. It has been studied as functions of centrality, transverse momentum, pseudorapidity (η), as well as the relations with the initial triangularity (ε_3) and shear viscosity over entropy density ratio [16–20]. However, the dependence of triangular flow on the elastic two-body partonic scattering cross section is absent. In addition, a possible NCQ-scaling, which has been found held by the elliptic flow [21], have not been studied in details for other v_n ($n=3,4,\dots$) when the initial fluctuations are taken into account.

This work presents the initial deformation scaling of elliptic (v_2), triangular (v_3) and quadrangular flows (v_4) for different cross sections within the framework of the AMPT model [22, 23]. The mass ordering at low p_T and constituent quark number scaling at higher p_T for the v_n are investigated after considering the event-by-event initial state geometry fluctuations at RHIC and LHC energies. Meanwhile, a special care is discussed for s -quark and ϕ meson for v_n -scaling.

The paper is organized in the following way. A brief description of the AMPT model is introduced in Sec. II. The results and discussions are presented in Sec. III. Finally, a summary is given in Sec. IV.

II. BRIEF DESCRIPTION OF AMPT MODEL

A multi-phase transport (AMPT) model consists of four main components: the initial condition, partonic interactions, conversion from partonic to hadronic matter, and hadronic interactions. The initial condition, which includes the spatial and momentum distributions of minijet partons and soft string excitations, is obtained from the Heavy Ion Jet Interaction Generator (HIJING) model. Scatterings among partons are modeled by Zhang’s Parton Cascade (ZPC) model, which includes

*Author to whom all correspondence should be addressed. Email: ygma@sinap.ac.cn

only two-body scatterings with cross sections obtained from the pQCD calculations with screening mass. In the default version of AMPT model, partons only include minijet partons, and recombine with their parent strings when they stop interactions, then the resulting strings are converted to hadrons by using the Lund string fragmentation mechanism. While in the version with the string melting mechanism, partons include minijet partons and partons from melted strings. And a quark coalescence model is used to combine partons into hadrons. The dynamics of the subsequent hadronic matter is then described by a relativistic transport (ART) model. Details of the AMPT model can be found in a review [23]. Previous AMPT calculations have found that elliptic flow can be built by strong parton cascade [23–26] and jet losses energy into partonic medium to excite an away-side double-peak structure [18, 27, 28]. Therefore, partonic effect can not be neglected and the string melting AMPT version is much more appropriate than the default version when the energy density is much higher than the predicted critical density. In this work, we use the version of AMPT model with the string melting mechanism to simulate Au+Au collisions at $\sqrt{s_{NN}} = 200$ GeV as well as Pb + Pb collisions at $\sqrt{s_{NN}} = 2.76$ TeV. Since collective flow has been built up after the expansion of partonic stage, we neglect the final hadronic rescattering effects on harmonic flows in this work.

III. RESULTS AND DISCUSSIONS

A. Brief definition of v_n with initial fluctuations

We know harmonic flows are defined as the n -th Fourier coefficient v_n of the particle distribution with respect to the reaction plane. However, after considering event-by-event fluctuations in the initial density distribution [16], the particle distribution should be written as

$$\frac{dN}{d\phi} \propto 1 + 2 \sum_{n=1}^{\infty} v_n \cos[n(\phi - \psi_n)], \quad (1)$$

where ϕ is the momentum azimuthal angle of each hadron. ψ_n is the n -th event plane which varies due to event-by-event fluctuations and can be calculated by

$$\psi_n^r = \frac{1}{n} \left[\arctan \frac{\langle r^2 \sin(n\varphi) \rangle}{\langle r^2 \cos(n\varphi) \rangle} + \pi \right], \quad (2)$$

where r and φ are the coordinate position and azimuthal angle of each parton and the average $\langle \dots \rangle$ is density weighted in the initial state, and the superscript r denotes initial coordinate space. The n -th order eccentricity ϵ_n for initial geometric distribution is defined as

$$\epsilon_n = \frac{\sqrt{\langle r^2 \cos(n\varphi) \rangle^2 + \langle r^2 \sin(n\varphi) \rangle^2}}{\langle r^2 \rangle}. \quad (3)$$

There is some arbitrariness in the definition of $\psi_n(r)$ and ϵ_n [29], because one could, for instance, replace r^2 with r^n in Eq. (2) and (3) [30]. With this replacement, however, v_3 and v_4 only change little in our calculations (less than 3% for v_3 and 12% for v_4 , respectively, for 0–80% centrality). In the following calculations, we will use Eq.(2) and Eq.(3) to decide ψ_n and ϵ_n .

After ψ_n is determined, the n -th harmonic flow v_n can be obtained by

$$v_n^r = \langle \cos[n(\phi - \psi_n^r)] \rangle. \quad (4)$$

In alternative way, ψ_n and v_n can be also calculated in momentum space as,

$$\psi_n^p = \frac{1}{n} \left[\arctan \frac{\langle p_T \sin(n\phi) \rangle}{\langle p_T \cos(n\phi) \rangle} \right], \quad (5)$$

and

$$v_n^p = \langle \cos[n(\phi - \psi_n^p)] \rangle, \quad (6)$$

where p_T and ϕ are the transverse momentum and azimuthal angle of each hadron, respectively, which is selected from pseudorapidity $|\eta| > 1$ in the final state to avoid autocorrelation, and the superscript p denotes final momentum space.

For v_n^p determined by the final momentum phase space, we can *even-by-event* correct v_n^p into v_n^r by

$$v_n^r = \left\langle \frac{v_n^{p,(e)} - s_n^{r,(e)} \sin[n(\psi_n^{p,(e)} - \psi_n^{r,(e)})]}{R_n^{(e)}} \right\rangle, \quad (7)$$

where the superscript (e) denotes "event-wise", $R_n^{(e)} = \cos[n(\psi_n^{p,(e)} - \psi_n^{r,(e)})]$ is event-wise event plane resolution, and $s_n^{r,(e)} = \sin[n(\phi - \psi_n^{r,(e)})]$ is event-wise \sin -term harmonic coefficient. We found that the contribution from \sin -term is only approximately 10%, therefore we neglect the \sin -term and correct v_n^p into v_n^r by $v_n^r = \langle v_n^{p,(e)} / R_n^{(e)} \rangle$, which is more operable experimentally.

It is essential to check if the $v_n(p_T)$ calculated by different ψ_n defined in coordinate space and momentum space is similar or not, because the determination of ψ_n^r in coordinate space by the Eq.(2) is not accessible in experiment. The p_T dependences of v_2 and v_3 with respect to ψ_n determined by initial coordinate and final momentum spaces are shown in Figure 1 together with the PHENIX v_2 data [31]. We observed that v_2 and v_3 determined by the final momentum space is very close to the ones with respect to initial coordinate space. (Note: we check that the differences are due to \sin -term contributions in event-by-event resolution corrections.) Also, the values can basically fit the PHENIX data, especially at low p_T .

Based upon the above observations on v_2 and v_3 with different phase space methods, we conclude that they basically can present the same results. Therefore in our following calculations, we apply the initial coordinate space to calculate ψ_n^r and then obtain the corresponding v_n .

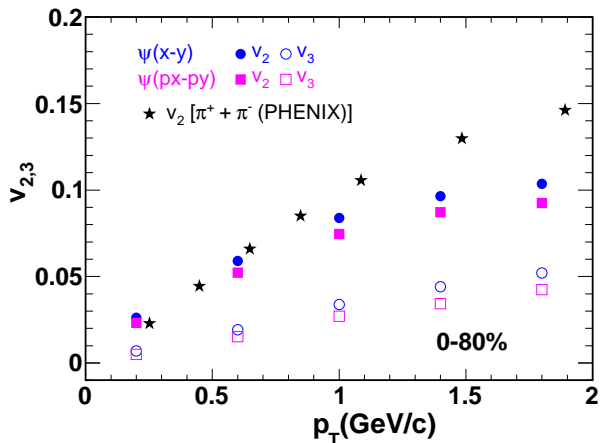


FIG. 1: (Color online) Comparison for v_2 (solid symbols) and v_3 (open symbols) calculated by $\psi_{2,3}^x$ defined in coordinate space (circles) or $\psi_{2,3}^p$ momentum space (squares) in Au + Au collisions (0-80% centrality) at $\sqrt{s_{NN}} = 200$ GeV from the AMPT simulation (3 mb). Note that v_2 and v_3 defined in momentum space (squares) have been even-by-event corrected by the event plane resolution. The PHENIX data are shown by solid stars [31].

B. Initial fluctuations and ratio of v_n/ε_n

The ratio of elliptic flow to eccentricity (v_2/ε_2) has been found to be sensitive to the freeze-out dynamics, the equation of state (EOS) and viscosity, however, v_3/ε_3 can give more information [16, 32–36]. Figure 2 shows the initial n -th order eccentricity ε_n and final harmonic flow v_n ($n = 2, 3$ and 4) in mid-rapidity as a function of impact parameter for Au + Au collisions at $\sqrt{s_{NN}} = 200$ GeV from the AMPT model simulations. The elastic two-body scattering cross section in the parton cascade process is set to be 3 mb.

As presented in Figure 2, the n -th order eccentricity ε_n ($n = 2, 3$ and 4) increases with impact parameter. ε_2 is larger than ε_3 and ε_4 , except in very central collisions where ε_n looks similar to each other. It is consistent with the trend given by Lacey *et al.* who applied MC-Glauber model, but gave a little smaller magnitude for peripheral collisions [37]. On the other hand, the coefficients of anisotropic flow v_n ($n = 2, 3$ and 4) show rising and falling with impact parameter. Also, v_n has a larger magnitude for lower harmonic than higher harmonic.

Similarly, Figure 3 shows the initial geometry deformation ε_n ($n = 2, 3$ and 4) for Pb + Pb collisions at $\sqrt{s_{NN}} = 2.76$ TeV, which demonstrates very similar behaviors as the RHIC energy.

Once we have v_n and ε_n , we can discuss the ratio v_n/ε_n ($n = 2, 3$ and 4). Figure 4 shows impact parameter and partonic cross section dependences of v_n/ε_n for Au + Au collisions at $\sqrt{s_{NN}} = 200$ GeV. The value of ratios decreases with impact parameter, which implies that the conversion from the initial geometry asymmetry to fi-

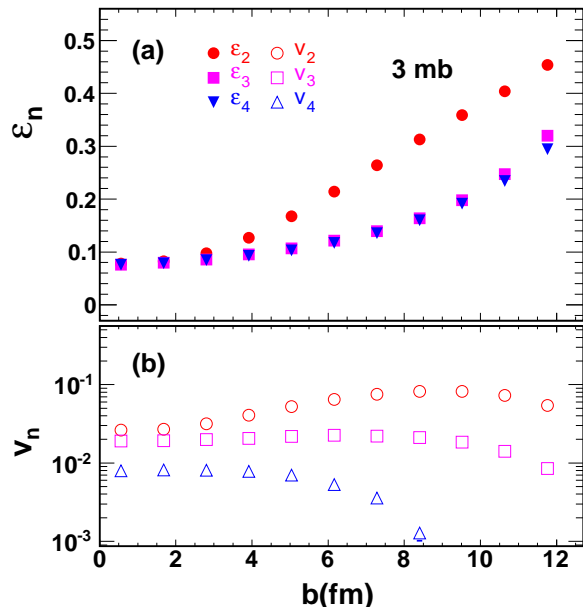


FIG. 2: (Color online) ε_n and v_n in mid-rapidity as functions of impact parameter for Au + Au collisions at $\sqrt{s_{NN}} = 200$ GeV from the AMPT simulation with partonic interaction cross section of 3 mb.

nal momentum anisotropy is less efficient for peripheral collisions than for central collisions. And for higher harmonics, there is also less conversion efficiency. The trend for v_n/ε_n as a function of impact parameter looks similar for the different partonic interaction cross sections of 3, 6 and 10 mb. However, the magnitude of v_n/ε_n decreases with the cross section, which reveals that the conversion from the initial geometry asymmetry to the final momentum anisotropy becomes weaker for a smaller cross section. This indicates that frequent parton-parton collisions help the system to develop the harmonic collectivity.

From Figure 4, we also saw that the v_n/ε_n becomes smaller for higher harmonic order, this may reflect the viscous damping. Recently, it was claimed that the relative magnitude of the higher-order harmonics ($v_n, n \geq 3$) can provide additional constraints on both the magnitude of η/s and the determination of initial condition [34, 37, 38]. Fig. 5 shows the n -dependence of v_n/ε_n for Au + Au collisions at $\sqrt{s_{NN}} = 200$ GeV and Pb + Pb collisions at $\sqrt{s_{NN}} = 2.76$ TeV for 0-20 % centrality and low p_T region ($p_T < 0.55$ GeV/c) (3 mb) with corresponding exponential fitting functions. Compared with PHENIX data, only the trend can be reproduced.

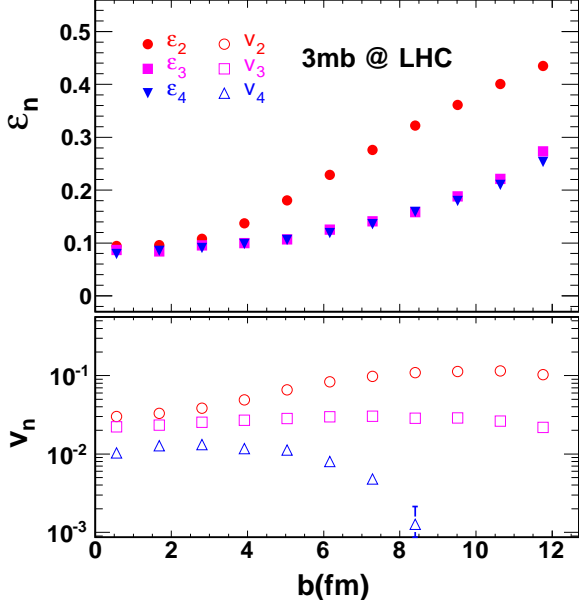


FIG. 3: (Color online) Same as Fig. 2 but for Pb + Pb collisions at $\sqrt{s_{NN}} = 2.76$ TeV.

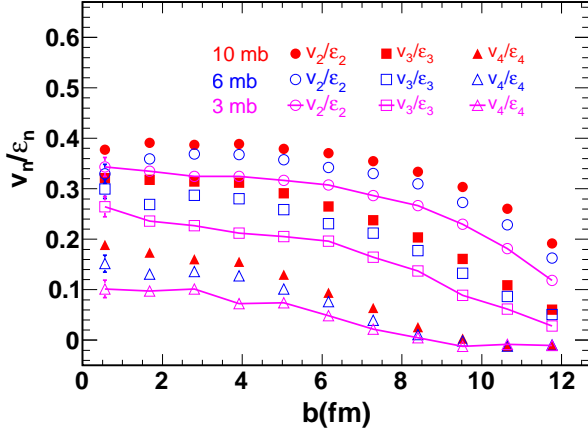


FIG. 4: (Color online) v_n/ϵ_n (circles for $n=2$, squares for $n=3$, and triangles for $n=4$) as a function of impact parameter for Au + Au collisions at $\sqrt{s_{NN}} = 200$ GeV in mid-rapidity for different parton interaction cross sections (10 mb, 6 mb and 3 mb).

C. p_T dependence of v_n with different partonic cross sections and comparisons with the data

Figure 6 presents our simulations of v_2 , v_3 and v_4 as a function of p_T with different parton interaction cross sections together with the PHENIX data [39]. For triangular flow, it totally arises from the event-by-event fluctuations of the initial collision geometry, because it persists zero if without considering the fluctuations. v_n

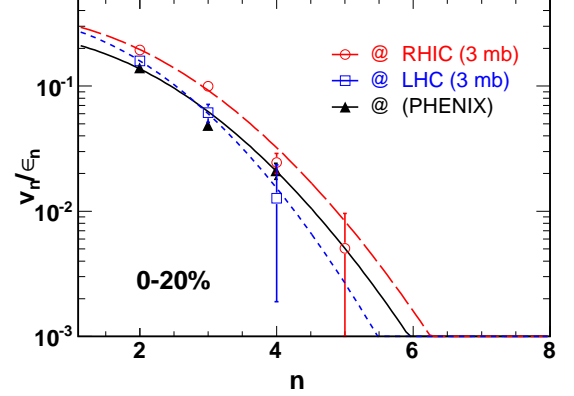


FIG. 5: (Color online) Harmonic order dependence of v_n/ϵ_n for Au + Au collisions at $\sqrt{s_{NN}} = 200$ GeV (circles) and Pb + Pb collisions at $\sqrt{s_{NN}} = 2.76$ TeV (squares) from the AMPT simulation (3 mb). PHENIX data are shown by triangles. The centrality is 0-20% and $p_T < 0.55$ GeV/c. The curves are exponential fitting functions.

($n = 2, 3$ and 4) decreases when parton-parton cross section decreases. Experimental data of v_2 can be described by the large cross sections (from 3 mb to 10 mb), after one considers of the initial fluctuations. However, the AMPT model underestimates the data if without taking the initial fluctuations into account. Recently, Xu and Ko adjusted more parameters in the AMPT model, which include not only parton interaction cross section but also the parametrization of the Lund string fragmentation, and found that a smaller cross section of 1.5 mb is good to describe both the charged particle multiplicity and elliptic flow [40]. In our work, we will not focus on how to further improve parameters, but we do find that initial geometry fluctuations significantly affect harmonic flows and should not be ignored.

The transverse momentum dependences of v_2 and v_3 with different cross sections in four different centrality bins are shown in Figure 7 and 8. The PHENIX data is also accompanied [41]. For each centrality bin, v_2 and v_3 increase with the cross section. For elliptic flow (Fig. 7), data seem to prefer a bigger cross section in higher transverse momentum range. In the case of triangular flow similar trend is present in Fig. 8, though v_3 shows a less centrality dependence than v_2 , which is consistent with the trends shown in Figure 2.

The transverse momentum dependences of v_2 and v_3 are also calculated for four different centrality bins in Pb + Pb collisions at $\sqrt{s_{NN}} = 2.76$ TeV for LHC energy, which are shown in Figure 9 and 10 together with the ATLAS data [42]. Similarly, v_2 and v_3 increase with the cross section from 3 mb to 10 mb, which can basically describe the ATLAS data.

Even though a general behavior of p_T -dependent v_n can be nicely demonstrated by the comparison of our calculations with the data, we found that the AMPT simula-

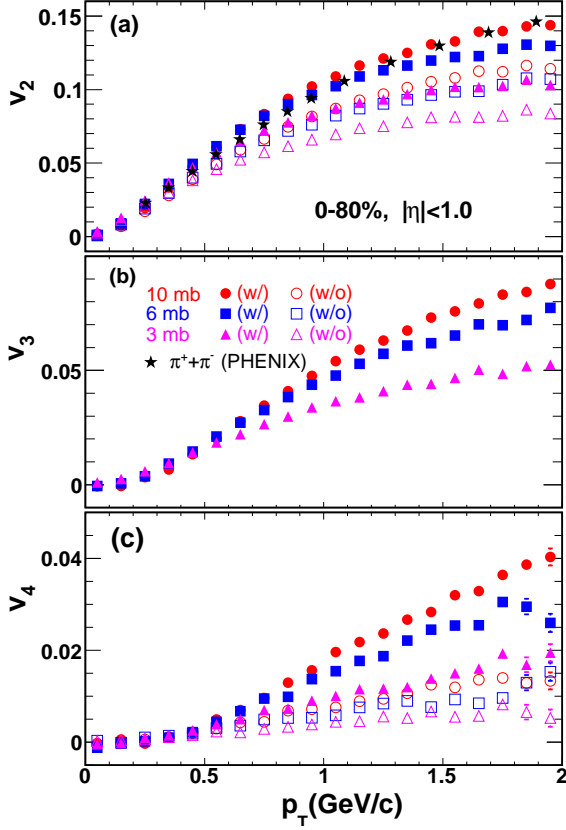


FIG. 6: (Color online) (a)-(c): Transverse momentum dependences of v_2 , v_3 , and v_4 for Au + Au collisions (0-80% centrality) at $\sqrt{s_{NN}} = 200$ GeV in mid-rapidity for different cross sections [10 mb (circle), 6 mb (square), and 3 mb (triangle)], where solid symbols are v_n with considering initial fluctuations and open symbols are those without considering initial fluctuations. The PHENIX data are shown by solid stars [39].

tions can only describe the trend of the data qualitatively. Actually, AMPT can not describe the v_2 and v_3 data simultaneously with a same cross section. For example, the 3mb results describe the v_2 and v_3 for 0-10% centrality but underpredict other centralities at RHIC energy. The 10mb data describe the v_2 for 10-20% centrality but are unable to reproduce v_3 for the same centrality. Also, the 10mb results describe the v_2 and v_3 for 30-40%, but underpredict the high p_T data for 50-60% centrality. For LHC data, no AMPT calculations can describe the v_2 and v_3 for the 0-10% centrality range.

D. NCQ-scaling of v_n at RHIC energy

For elliptic flow, a mass ordering (the heavier the hadron mass, the smaller the v_2) and a NCQ-scaling (baryon versus meson) have been observed at low and intermediate p_T , respectively, in Au + Au collisions at $\sqrt{s_{NN}} = 200$ GeV [43]. The observed NCQ-scaling

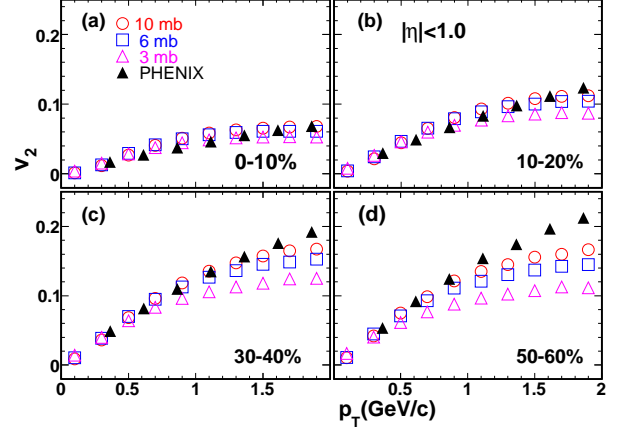


FIG. 7: (Color online) v_2 as a function of p_T in Au + Au collisions at $\sqrt{s_{NN}} = 200$ GeV for different centrality bins (0-10%, 10-20%, 30-40% and 50-60%) with different cross sections. Circles, squares and triangles represent the calculation with 10 mb, 6 mb and 3 mb, respectively. The PHENIX data shown by solid triangle [41].

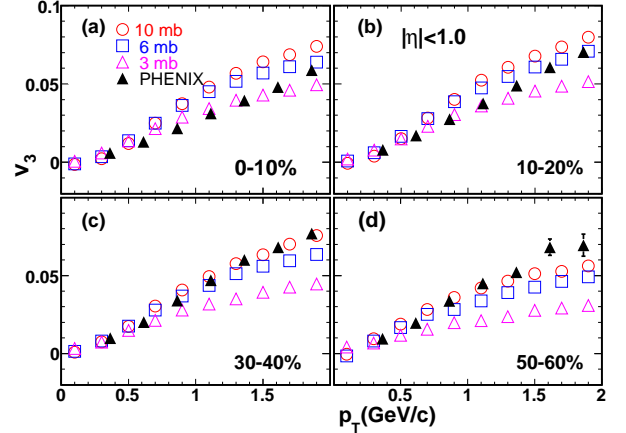


FIG. 8: (Color online) Same as Fig. 7 but for v_3 .

(v_2/n_q vs KE_T/n_q) reveals a universal scaling of v_2 for all identified particles over the full transverse kinetic energy (KE_T) range, which is more pronounced rather than p_T [3, 8–12, 44]. Such scaling indicates that the collective elliptic flow has been developed during the partonic stage and the effective constituent quark degree of freedom plays an important role in hadronization process. For higher even-order harmonics, v_4 and v_6 etc, appear to be scaled as $v_n \propto v_2^{n/2}$ [45] and their NCQ-scaling has also been suggested in Ref. [46]. Even in very low energy heavy ion collisions, the v_2 -scaling and the v_4/v_2^2 -scaling have been suggested for light nuclear clusters in nucleonic level interaction [47]. Instead scaling by the number of constituent quarks (n_q) for v_2 , the measured data v_4 , however, seems to be scaled by n_q^2 [21]. It is interesting

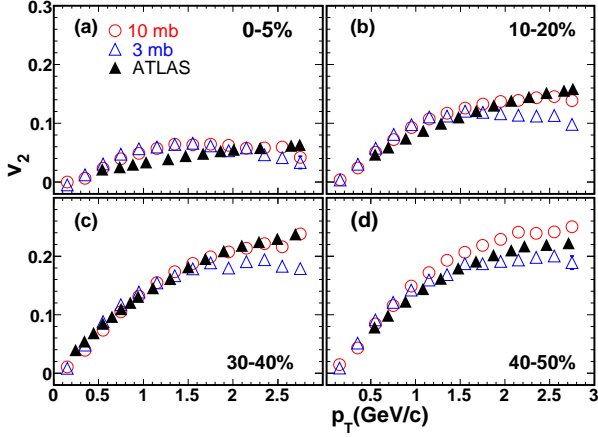


FIG. 9: (Color online) v_2 as a function of p_T in Pb + Pb collisions at $\sqrt{s_{NN}} = 2.76$ TeV from the AMPT simulations (3 mb and 10 mb) for different centrality bins (0-5%, 10-20%, 30-40%, and 40-50%) at midrapidity. Circles and triangles represent the calculations with 10 mb and 3 mb, respectively. The ATLAS data shown by solid triangles [42].

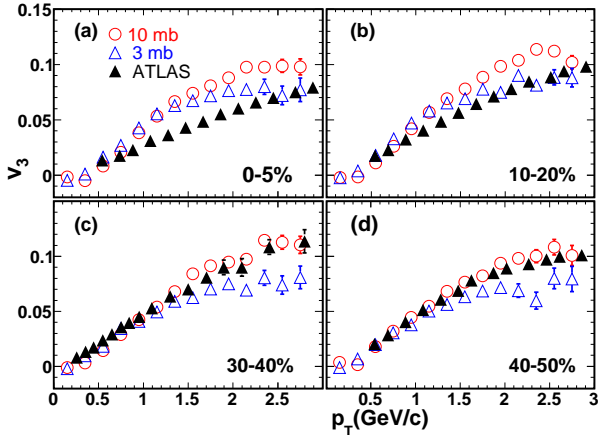


FIG. 10: (Color online) Same as Fig. 9 but for v_3 .

to check if these scaling relations are still valid for the v_n calculations in which the initial fluctuations are taken into account, including the odd harmonics, such as v_3 .

Figure 11 presents v_2 , v_3 and v_4 of different types of hadrons in mid-rapidity for Au + Au collisions (0-80% centrality) at $\sqrt{s_{NN}} = 200$ GeV. Figure 11 (a) shows that v_2 preserves an obvious mass ordering in relatively low p_T region, and hadron type grouping in intermediate p_T region, even after considering event-by-event fluctuations. Similarly, v_3 and v_4 , [Figure 11 (b) and (c)] also present a mass ordering in the low p_T region. The study on v_n of different hadron species will give more information about the initial geometry and the viscosity of hot and dense matter [34].

As shown in Figure 12(a), v_2 scaled by the number of

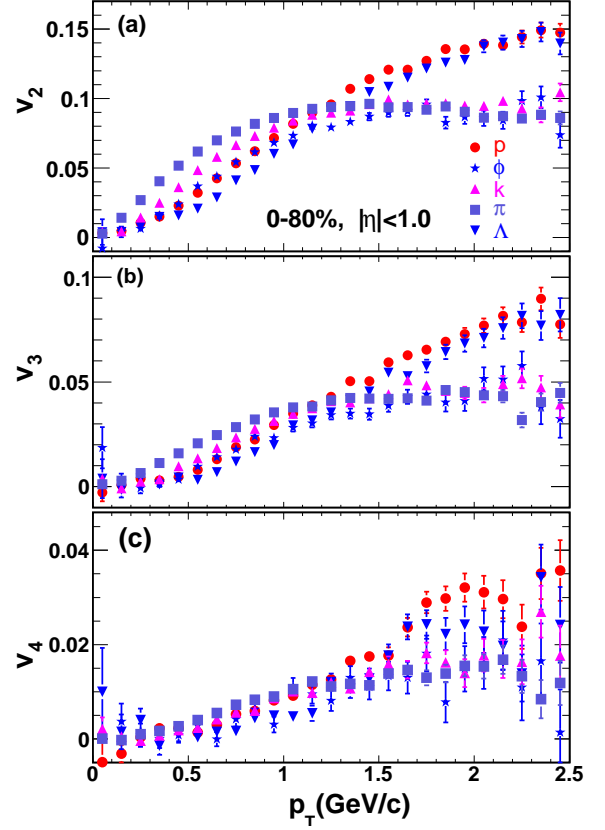


FIG. 11: (Color online) (a)-(c): Transverse momentum dependences of v_2 , v_3 , and v_4 for different hadron species in Au + Au collisions (0-80% centrality) at $\sqrt{s_{NN}} = 200$ GeV in mid-rapidity from the AMPT simulations (3 mb), with considering of initial fluctuations.

constituent quarks (v_2/n_q) as a function of the transverse kinetic energy ($KE_T = \sqrt{p_T^2 + m^2} - m$) scaled by the number of constituent quarks (KE_T/n_q) shows a universal scaling regardless of the initial geometry fluctuations are taken into consideration or not. The only difference is that the initial fluctuations enhance the value of v_2/n_q . Therefore, the initial fluctuations have little effect on the breaking of the NCQ-scaling for elliptic flow. Figure 12 (b) and (c) display $v_3/n_q^{3/2}$ and v_4/n_q^2 for all hadrons as a function of KE_T/n_q , respectively, when the initial fluctuations are considered. From the above results, it seems that v_n can still be roughly scaled by $n_q^{n/2}$ for all hadrons as a function of KE_T/n_q . Of course, the scaling behavior is not perfect within the present statistics. For example, the amount of spread between different particle species is less than 10% for the v_2 -scaling, it is less than 20% for the v_3 -scaling, but it can reach 20-30% for the v_4 -scaling.

In order to understand possible origin of the NCQ-scaling of v_n for different mesons and baryons, we also check v_n of u , d and s -quarks as a function of p_T or KE_T . As expected, there exists similar NCQ-scaling of

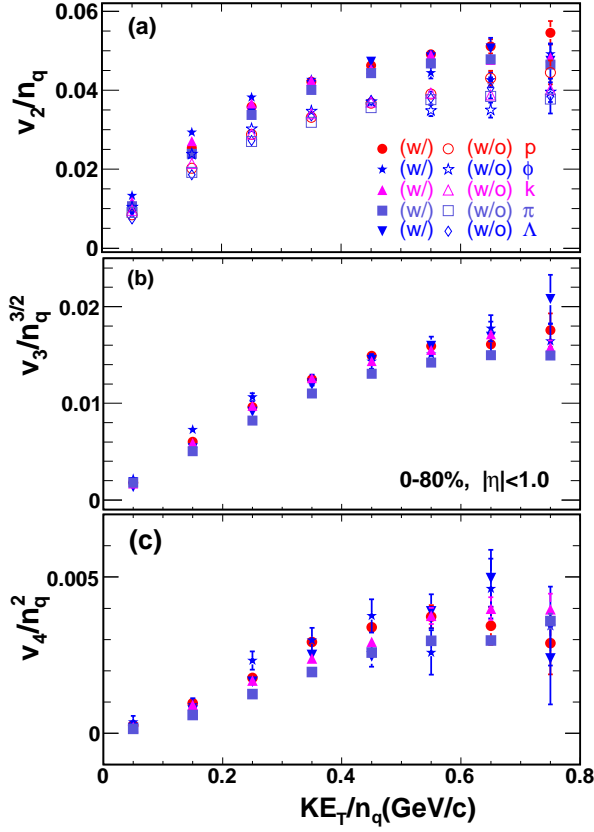


FIG. 12: (Color online) (a)-(c): v_2/n_q , $v_3/n_q^{3/2}$ and v_4/n_q^2 as a function of KE_T/n_q in Au + Au collisions (0-80% centrality) at $\sqrt{s_{NN}} = 200$ GeV from the AMPT simulations (3 mb), where the solid symbols are the results for considering initial fluctuations (w/), while the open ones are for without considering initial fluctuations (w/o).

v_n ($n=2-4$) for all those constituent quarks. Furthermore, we find that the values of $v_n/n_q^{n/2}$ of different hadrons are similar to the values of v_n of u, d, s -quarks, which reflects that the NCQ-scaling of v_n for different hadrons stems from partonic level.

Furthermore, the ratios of $v_3/v_2^{3/2}$ and v_4/v_2^2 as functions of p_T for three different centrality bins (10-20%, 20-30%, and 30-40%) in Au + Au collisions at $\sqrt{s_{NN}} = 200$ GeV are shown in Figure 13. It shows that the both ratios of $v_3/v_2^{3/2}$ [Figure 13 (a)] and v_4/v_2^2 [Figure 13 (b)] exhibit centrality dependences, i.e. more central collisions result in more larger ratios. However, it is almost independent of p_T for each centrality bin, which is consistent with the scaling of $v_n/n_q^{n/2}$ observed in Figure 12. However, it is difficult to obtain the relationship between $v_{n,q}$ and $v_{2,q}$, such as between v_3 and v_2 , in terms of a simple coalescence model in Ref. [48], because ψ_3 is purely determined by initial geometry fluctuations which is independent of ψ_2 . It is interesting that recently Lacey *et al.* linked such a scaling to the acoustic nature of anisotropic flow to constrain initial conditions, η/s and viscous hori-

zon [49]. It further gives more insights on the dynamics of strongly-interacting partonic matter and constituent quark degree of freedom in hadronization process.

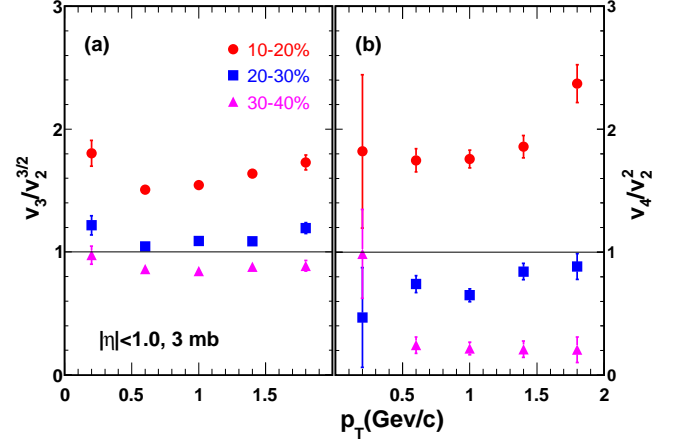


FIG. 13: (Color online) The ratios of $v_3/v_2^{3/2}$ (a) and v_4/v_2^2 (b) as a function of p_T for three different centrality bins (10-20%, 20-30%, and 30-40%) in Au + Au collisions at $\sqrt{s_{NN}} = 200$ GeV from the AMPT simulations (3 mb).

E. NCQ-scaling of v_n at LHC energy

At the same time, the mass ordering in the low p_T region and the NCQ-scaling in intermediate p_T region of v_n are also investigated at LHC energy in AMPT simulations. Fig. 14 presents the results of v_2 , v_3 , and v_4 for different hadron species in Pb + Pb collisions (0-80% centrality) at $\sqrt{s_{NN}} = 2.76$ TeV in mid-rapidity from the AMPT calculations (3 mb), with considering initial fluctuations. It displays that the mass ordering is satisfied, i.e. v_n decreases from π , k , p , ϕ to Λ in the lower p_T region (note that ϕ is very close to p in the figure). However, the strict mass-ordering needs ϕ 's v_n is little less than p 's v_n). The baryon-meson typing is also evident above $p_T \sim 1.2$ GeV. By transformation of p_T to KE_T/n_q as well as v_n to $v_n/n_q^{n/2}$, the results of v_2/n_q , $v_3/n_q^{3/2}$ and v_4/n_q^2 as a function of KE_T/n_q are shown in Fig. 15. Again, the NCQ-scaling of v_n is roughly kept except for ϕ meson whose v_n is a little larger. Of course, the amount of spread between different particle species for v_n -scaling keeps similar as RHIC energy. Comparing with the above v_n results at RHIC, LHC results are very similar but they reveal larger v_n values than RHIC's due to stronger partonic interactions at higher energy. But in general, the partonic matter formed at LHC energy is very similar to that created at RHIC energy.

As mentioned above, ϕ -meson shows a little larger value of $v_n/n_q^{n/2}$ as compared to those of other hadrons in Fig. 15. Keep in mind that ϕ -meson is always a very interesting hadron in previous studies since its mass is close

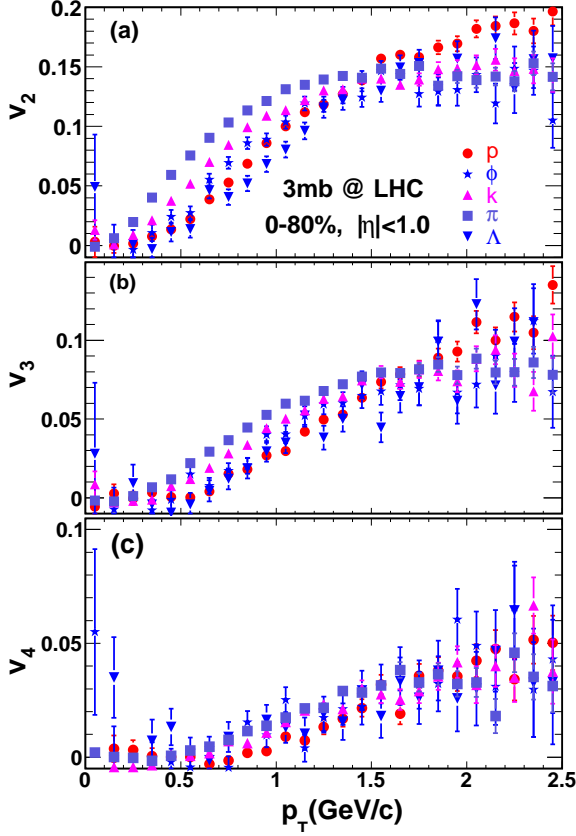


FIG. 14: (Color online) (a)-(c): The transverse momentum dependences of v_2 , v_3 , and v_4 for different hadron species in Pb + Pb collisions (0-80% centrality) at $\sqrt{s_{NN}} = 2.76$ TeV in mid-rapidity from the AMPT simulations (3 mb), with considering initial fluctuations.

to proton but it is a multi-strange meson [3, 50–54]. This could be understood from the parton's v_n in the same condition: v_n of s -quark displays a slight deviation from the u (d)-quarks (not shown here). The reason could be that the v_n of heavier strange quarks has a smaller value at low p_T but a larger value at high p_T , i.e. the mass ordering of partonic flow. However, a larger collective radial flow at LHC energy could push heavier s -quark to have stronger v_n . The effect is of course more distinct at LHC energy because of larger initial partonic pressure. In contrast, in low energy RHIC run, such as 11.5 GeV/c Au + Au collision, s -quark may not reach full thermalization and therefore result in a less v_2 of s -quark as compared to $u(d)$ -quarks, which can lead to a smaller v_2 of ϕ , i.e. the violation of the v_2 -scaling for the ϕ -mesons relative to other hadrons as observed in the STAR data [54] as well as in a simulation [12]. Considering that the ϕ -meson is coalesced by $s\bar{s}$ in the present AMPT model calculation, it will certainly induce a larger $v_n/n_q^{n/2}$ for ϕ in comparison with other hadrons, as shown in Fig. 15. Unfortunately, the data of ϕ 's v_n is not available yet at LHC energy, which is worth waiting for checking.

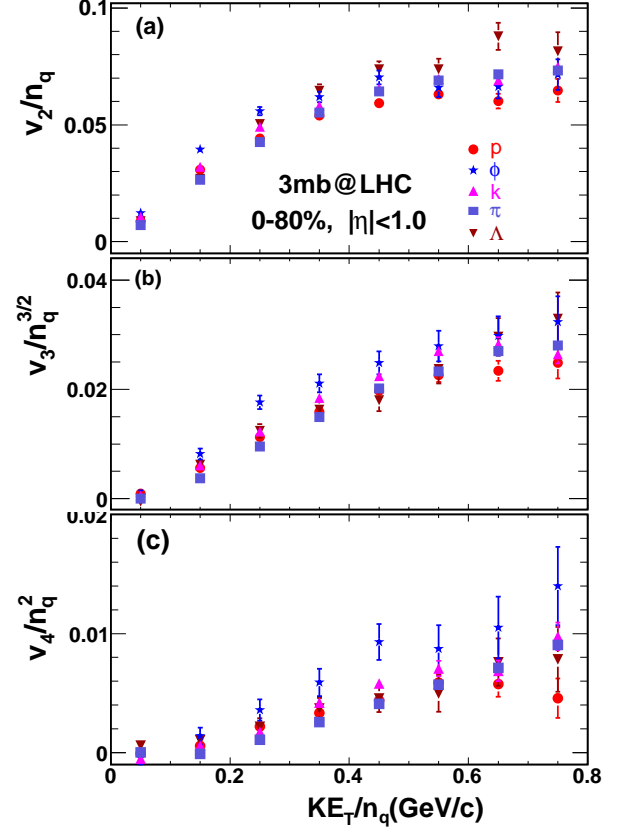


FIG. 15: (Color online) (a)-(c): v_2/n_q , $v_3/n_q^{3/2}$ and v_4/n_q^2 as a function of KE_T/n_q in Pb + Pb collisions (0-80% centrality) at $\sqrt{s_{NN}} = 2.76$ TeV from the AMPT simulations (3 mb).

Before closing the discussions on the NCQ-scaling of v_n in this subsection, we remind that the hadronic rescattering process is not yet taken into account in our calculation. Recently, the ALICE data shows that proton's v_2 and v_3 seem to deviate from the NCQ-scaling of v_n of charged π and K [55]. The reason could be stronger final-state interaction for protons. Detailed model investigations are underway.

IV. SUMMARY

Within the framework of a multi-phase transport model, we investigated the different orders of harmonic flows, namely elliptic flow, triangular flow and quadrangular flow for Au + Au collisions at $\sqrt{s_{NN}} = 200$ GeV as well as Pb + Pb collisions at $\sqrt{s_{NN}} = 2.76$ TeV when the initial geometry fluctuations are taken into account. Basically, the harmonic flow is converted from initial geometry shape via parton cascade process, and its conversion efficiency (v_n/ε_n) decreases with the increasing of harmonic order as well as the decreasing of the partonic cross section at both RHIC and LHC energies. Dependences of transverse momentum, centrality and partonic

cross section of the v_n ($n=2, 3$ and 4) have been studied and compared with data. For each centrality bin, v_2 and v_3 increases with cross section, especially at higher transverse momentum.

Triangular and quadrangular flows also roughly present a mass ordering in low p_T region and the number of constitute quark scaling in intermediate p_T region, similar to the behaviors of elliptic flow. Form our results, a NCQ-scaling of $v_n/n_q^{n/2}$ versus KE_T/n_q for different hadrons holds for harmonic flow ($v_n, n = 2, 3$ and 4), which can be related to v_n -scaling in partonic level. From all above results, it implies that the formed partonic matter should be very similar for RHIC and LHC energies.

Acknowledgements

The authors thank Dr. B. Johnson, and Dr. S. Esumi for providing data kindly. The authors also thank Dr. M. Luzum, Dr. J. Y. Ollitrault, Dr. Y. Zhou and Dr. R. Lacey for helpful discussion. This work was supported in part by the National Natural Science Foundation of China under contract Nos. 11035009, 11005140, 11175232, 10979074, 10875159 and the Knowledge Innovation Project of the Chinese Academy of Sciences under Grant No. KJCX2-EW-N01, and the Project-sponsored by SRF for ROCS, SEM.

-
- [1] I. Arsene *et al.* (BRAHMS Collaboration), Nucl. Phys. A **757**, 1 (2005); B. B. Back *et al.* (PHOBOS Collaboration), Nucl. Phys. A **757**, 28 (2005); J. Adams *et al.* (STAR Collaboration), Nucl. Phys. A **757**, 102 (2005); S. S. Adcox *et al.* (PHENIX Collaboration), Nucl. Phys. A **757**, 184 (2005).
 - [2] S. A. Voloshin, A. M. Poskanzer, and R. Snellings, arXiv:0809.2949.
 - [3] J. H. Chen, Y. G. Ma, G. L. Ma, X. Z. Cai, Z. J. He, H. Z. Huang, J. L. Long, W. Q. Shen, C. Zhong, J. X. Zuo, Phys. Rev. C **74**, 064902 (2006).
 - [4] L. P. Csernai, J. I. Kapusta, and L. D. McLerran, Phys. Rev. Lett. **97**, 152303 (2006).
 - [5] R. A. Lacey, N. N. Ajitanand, J. M. Alexander, P. Chung, W. G. Holzmann, M. Issah, and A. Taranenko, Phys. Rev. Lett. **98**, 092301 (2007).
 - [6] Huichao Song, Steffen A. Bass, Ulrich Heinz, Tetsufumi Hirano, and Chun Shen, Phys. Rev. Lett. **106**, 192301 (2011).
 - [7] R. Peschanski, E. N. Saridakis, Phys. Rev. C **80**, 024907, 2009
 - [8] J. Adams *et al.* (STAR Collaboration), Phys. Rev. Lett. **95**, 122301 (2005).
 - [9] J. Adams *et al.* (STAR Collaboration), Phys. Rev. Lett. **92**, 052302 (2004).
 - [10] A. Adare *et al.* (PHENIX Collaboration), Phys. Rev. Lett. **98**, 162301 (2007).
 - [11] S. Afanasiev *et al.* (PHENIX Collaboration), Phys. Rev. Lett. **99**, 052301 (2007).
 - [12] J. Tian, J. H. Chen, Y. G. Ma, X. Z. Cai, F. Jin, G. L. Ma, S. Zhang, and C. Zhong, Phys. Rev. C **79**, 067901 (2009).
 - [13] P. Sorensen, arXiv:1002.4878; P. Sorensen, B. Bolliet, A. Mocsy, Y. Pandit, N. Pruthi, arXiv:1102.1403; A. Mocsy, P. Sorensen, arXiv:1008.3381.
 - [14] B. Alver *et al.*, Phys. Rev. Lett. **98**, 242302 (2007).
 - [15] B. Alver *et al.* (PHOBOS Collaboration), Phys. Rev. C **81**, 034915 (2010).
 - [16] B. Alver and G. Roland, Phys. Rev. C **81**, 054905 (2010).
 - [17] J. Xu, C. M. Ko, Phys. Rev. C **83**, 021903 (2011).
 - [18] G. L. Ma and X. N. Wang, Phys. Rev. Lett. **106**, 162301 (2011).
 - [19] H. Petersen, G. Y. Qin, S. Bass, and B. Müller, Phys. Rev. C **82**, 041901(R) (2010).
 - [20] G. Y. Qin, H. Petersen, S. Bass, and B. Müller, Phys. Rev. C **82**, 064903 (2010).
 - [21] S. Huang (for the PHENIX Collaboration), J. Phys. G **35**, 104105, (2008).
 - [22] B. Zhang, C. M. Ko, B. A. Li, and Z. W. Lin, Phys. Rev. C **61**, 067901 (2000).
 - [23] Z. W. Lin, Che Ming Ko, Bao-An Li, Bin Zhang, Subrata Pal, Phys. Rev. C **72**, 064901 (2005).
 - [24] Z. W. Lin, C. M. Ko, Phys. Rev. C **65**, 034904 (2002).
 - [25] Md. Nasim, L. Kumar, P. K. Netrakanti, B. Mohanty, Phys. Rev. C **82**, 054908 (2010); C. M. Ko, L.-W. Chen, Nucl. Phys. A **774**, 527 (2006); B. Zhang, L.-W. Chen, C. M. Ko, Nucl. Phys. A **774**, 665 (2006).
 - [26] J. Xu, C. M. Ko, Phys. Rev. C **83**, 034904 (2011).
 - [27] G. L. Ma, S. Zhang, Y. G. Ma, H. Z. Huang, X. Z. Cai, J. H. Chen, Z. J. He, J. L. Long, W. Q. Shen, X. H. Shi, J. X. Zuo, Phys. Lett. B **641**, 362 (2006).
 - [28] H. L. Li, F. M. Liu, G. L. Ma, X. N. Wang, Y. Zhu, Phys. Rev. Lett. **106**, 012301 (2011).
 - [29] B. H. Alver, C. Gombeaud, M. Luzum, and J.-Y. Ollitrault, Phys. Rev. C **82**, 034913 (2010).
 - [30] D. Teaney, presented at Strong and Electroweak Matter 2010, Montreal, Canada, June 29/July 2.
 - [31] A. Adare *et al.* (PHENIX Collaboration), Phys. Rev. Lett. **98**, 162301 (2007).
 - [32] Z. Qiu and U. Heinz, Phys. Rev. C **84**, 024911 (2011).
 - [33] B. Schenke, S. Jeon, and C. Gale, Phys. Rev. Lett. **106**, 042301 (2011).
 - [34] B. H. Alver, C. Gombeaud, M. Luzum, J. Y. Ollitrault, Phys. Rev. C **82**, 034913 (2010).
 - [35] M. Issah, A. Taranenko, arXiv:nucl-ex/0604011.
 - [36] D. Teaney, Li Yan, Phys. Rev. C **83**, 064904 (2011).
 - [37] R. A. Lacey, Rui Wei, N. N. Ajitanand, A. Taranenko, Phys. Rev. C **83**, 044902 (2011).
 - [38] P. Staig and E. Shuryak, Phys. Rev. C **84**, 034908 (2011).
 - [39] A. Adare *et al.* (PHENIX Collaboration), Phys. Rev. Lett. **98**, 162301 (2007).
 - [40] J. Xu, C. M. Ko, Phys. Rev. C **84**, 014903 (2011).
 - [41] A. Adare *et al.* (PHENIX Collaboration), aXiv:1105.3928.
 - [42] J. Jia (for the ATLAS Collaboration), J. Phys. G **38**, 124012 (2011).
 - [43] J. Adams *et al.* (STAR Collaboration), Phys. Rev. C **72**, 014904 (2005).

- [44] B. I. Abelev *et al.* (STAR Collaboration), Phys. Rev. C **77**, 054901 (2008).
- [45] J. Adams *et al.* (STAR collaboration), Phys. Rev. Lett. **92**, 062301 (2004).
- [46] D. Molnar and S. A. Voloshin, Phys. Rev. Lett. **91**, 092301 (2003).
- [47] T. Z. Yan, Y. G. Ma, X. Z. Cai, J. G. Chen, D. Q. Fang, W. Guo, C. W. Ma, E. J. Ma, W. Q. Shen, W. D. Tian and K. Wang, Phys. Lett. B **638**, 50 (2006); T. Z. Yan, Y. G. Ma, X. Z. Cai, D. Q. Fang, W. Guo, C. W. Ma, W. Q. Shen, W. D. Tian, and K. Wang, Chin. Phys. **16**, 2676 (2007).
- [48] P. F. Kolb, L. W. Chen, V. Greco, C. M. Ko, Phys. Rev. C **69**, 051901 (2004).
- [49] R. A. Lacey, A. Taranenko, N. N. Ajitanand, J. M. Alexander, arXiv:1105.3782.
- [50] Y. G. Ma, J. Phys. G **32**, S373 (2006).
- [51] B. I. Abelev *et al.* (STAR Collaboration), Phys. Rev. Lett. **99**, 112301 (2007).
- [52] B. I. Abelev *et al.* (STAR Collaboration), Phys. Rev. C **77**, 061902(R) (2008).
- [53] B. I. Abelev *et al.* (STAR Collaboration), Phys. Rev. C **79**, 064903 (2009).
- [54] B. Mohanty (for the STAR Collaboration), J. Phys. G **38** 124023 (2011).
- [55] M. Krzewicki (for the ALICE Collaboration), J. Phys. G **38** 124047 (2011).